Copy No. 11

DEFENCE R&D DÉFENSE

VERTICAL COHERENCE OF THE SHALLOW WATER AMBIENT NOISE FIELD, A MODEL

F. Desharnais – D.M.F. Chapman

DEFENCE RESEARCH ESTABLISHMENT ATLANTIC

Technical Memorandum

DREA TM 1999-011

February 1999

National Defence Défense nationale

Canada

National Defence
Research and Development Branch

Défense nationale
Bureau de recherche et développement

DREA TM 1999-011

Vertical Coherence of the Shallow Water Ambient Noise Field, a Model

F. Deshamais – D.M.F. Chapman

DEFENCE RESEARCH ESTABLISHMENT ATLANTIC
PO Box 1012, Dartmouth
Nova Scotia, Canada
B2Y 3Z7

Approved by
J.S. Kennedy
Head, Underwater Acoustics Section
February 1999

TECHNICAL MEMORANDUM

Prepared by

Defence Research Establishment Atlantic

Centre de Recherches pour la Défense Atlantique

Canada

102-02850/

DREA TM 1999-011

Vertical coherence of the shallow water ambient noise field, a model

Francine Desharnais and David M.F. Chapman

EXECUTIVE SUMMARY

Introduction

The use of ambient noise to extract environmental information is particularly advantageous since it is ever-present in the ocean. It has already been shown in the open literature that some seabed properties can be successfully extracted from the spatial characteristics of the ambient noise field, either from its vertical directionality or its vertical coherence. So far, the technique has worked best for properties of the surficial sediment, for example the compressional and shear speed at the sediment surface.

Chapman [Proc. Inst. of Acoust., 1987, 9(4), 1-11] developed a model to estimate the vertical ambient noise coherence in a simple shallow water environment. This report restates the original equations of the model, and extends it to include a multi-layered elastic seabed, sea water absorption, and an arbitrary sound speed profile in the water column. Also included is a sensitivity study of the model to the following internal parameters: absorption by sea water, bottom parameters, sound speed profile in the water column, and source directivity.

Principal Results

The model is based on an energy flux propagation model, and is very simple in its formulation. Most effects from the ocean and seabed, other than range-dependence, are included in the model without having recourse to the full wave equation; yet the model leads to realistic results for a very modest computational cost.

The sensitivity study showed that the compressional sound speed of the upper sediment layer has a strong influence on the vertical noise coherence, as does the shear speed, if high. Compressional and shear wave attenuations as well as density have lesser effects. Sediment layering can also induce large changes in the vertical coherence. The coherence becomes less sensitive to seabed properties below a few tens of meters within the seabed.

The coherence is a normalized measurement, therefore the structure of the noise coherence is more sensitive to the seabed properties than to sea state conditions (for those frequencies where the main noise source is due to surface agitation). However, the sound speed profile in the water column, as in the seabed, has a directional effect on the noise spatial distribution, and can be very important, especially for upward-refracting profiles when bottom interactions are limited. Poor knowledge of the oceanographic environment can lead to poor estimates of seabed parameters.

Shipping effects were not modelled directly, but it was demonstrated that it might be possible to mimic distant shipping by increasing the source level at near-horizontal angles.

Military Relevance

In shallow water, sonar performance is strongly affected by the acoustic characteristics of the seafloor. Knowledge of these characteristics can be used to improve sonar performance indirectly, by suggesting changes in the use of the sonar, or directly, through inclusion in the processing applied to the recorded signals.

There exist several methods to determine bottom properties from simple acoustic measurements. The use of noise coherence has several strong advantages. First, ambient noise is always present in the ocean, and the method should work independently of the amplitude of the backgound noise levels. Second, the vertical coherence measurement is relatively easy to make as it requires only two vertically separated sensors, as opposed to a directionality measurement which requires several more sensors. A sonobuoy-type device would be relatively easy to make for such a measurement. Third, the method is fast, does not require a sonar source, and potentially gives valuable environmental information for sonar operations. These advantages make the method worth investigating.

Future Work

The obvious continuation of this work is a trial of the technique with actual measurements of vertical noise coherence. For this purpose, data have already been collected at a few sites on the Scotian Shelf, mainly at Western Bank. Model-data comparisons, as well as an evaluation of the method will be presented in a future report.

ABSTRACT

A shallow water noise model is used to simulate the vertical coherence of an acoustic noise field due to sea surface noise. The coherence between two vertically separated sensors is calculated from the Fourier transform of the received noise intensity as a function of vertical arrival angle. The vertical noise directionality is derived from a uniform distribution of sources at the ocean surface, an energy flux propagation model and a plane-wave bottom reflection coefficient for a multi-layered elastic seabed. The propagation model allows for an arbitrary sound speed profile in the water column and includes sea water absorption. This simple model clearly demonstrates the influence of seabed parameters, sound speed profile in the water, and noise source directivity on the vertical coherence of the noise field.

RÉSUMÉ

Un modèle de bruit en eau peu profonde est utilisé pour simuler la cohérence verticale d'un champ de bruit acoustique attribuable au bruit de surface de la mer. La cohérence entre deux capteurs séparés verticalement est calculée à l'aide de transformées de Fourier de l'intensité du bruit reçu en fonction de l'angle d'arrivée vertical. La directivité verticale du bruit est dérivée d'une distribution uniforme des sources à la surface de l'océan, d'un modèle de propagation du flux d'énergie et d'un coefficient de réflexion pour onde plane pour un plancher océanique élastique multicouches. Le modèle de propagation prévoit un profil de vitesse du son arbitraire dans la colonne d'eau et tient compte de l'absorption de l'eau de mer. Ce modèle simple démontre clairement l'influence des paramètres du plancher océanique, du profil de la vitesse du son dans l'eau et de la directivité de la source de bruit sur la cohérence verticale du champ de bruit.

DREA TM 1999-011

Vertical coherence of the shallow water ambient noise field, a model

Francine Desharnais and David M.F. Chapman

EXECUTIVE SUMMARY

Introduction

The use of ambient noise to extract environmental information is particularly advantageous since it is ever-present in the ocean. It has already been shown in the open literature that some seabed properties can be successfully extracted from the spatial characteristics of the ambient noise field, either from its vertical directionality or its vertical coherence. So far, the technique has worked best for properties of the surficial sediment, for example the compressional and shear speed at the sediment surface.

Chapman [*Proc. Inst. of Acoust.*, 1987, 9(4), 1-11] developed a model to estimate the vertical ambient noise coherence in a simple shallow water environment. This report restates the original equations of the model, and extends it to include a multi-layered elastic seabed, sea water absorption, and an arbitrary sound speed profile in the water column. Also included is a sensitivity study of the model to the following internal parameters: absorption by sea water, bottom parameters, sound speed profile in the water column, and source directivity.

Principal Results

The model is based on an energy flux propagation model, and is very simple in its formulation. Most effects from the ocean and seabed, other than range-dependence, are included in the model without having recourse to the full wave equation; yet, the model leads to realistic results for a very modest computational cost.

The sensitivity study showed that the compressional sound speed of the upper sediment layer has a strong influence on the vertical noise coherence, as does the shear speed, if high. Compressional and shear wave attenuations as well as density have lesser effects. Sediment layering can also induce large changes in the vertical coherence. The coherence becomes less sensitive to seabed properties below a few tens of meters within the seabed.

The coherence is a normalized measurement, therefore the structure of the noise coherence is more sensitive to the seabed properties than to sea state conditions (for those frequencies where the main noise source is due to surface agitation). However, the sound speed profile in the water column, as in the seabed, has a directional effect on the noise spatial distribution, and can be very important, especially for upward-refracting profiles when bottom interactions are limited. Poor knowledge of the oceanographic environment can lead to poor estimates of seabed parameters.

Shipping effects were not modelled directly, but it was demonstrated that it might be possible to mimic distant shipping by increasing the source level at near-horizontal angles.

Military Relevance

In shallow water, sonar performance is strongly affected by the acoustic characteristics of the seafloor. Knowledge of these characteristics can be used to improve sonar performance indirectly, by suggesting changes in the use of the sonar, or directly, through inclusion in the processing applied to the recorded signals.

There exist several methods to determine bottom properties from simple acoustic measurements. The use of noise coherence has several strong advantages. First, ambient noise is always present in the ocean, and the method should work independently of the amplitude of the backgound noise levels. Second, the vertical coherence measurement is relatively easy to make as it requires only two vertically separated sensors, as opposed to a directionality measurement which requires several more sensors. A sonobuoy-type device would be relatively easy to make for such a measurement. Third, the method is fast, does not require a sonar source, and potentially gives valuable environmental information for sonar operations. These advantages make the method worth investigating.

Future Work

The obvious continuation of this work is a trial of the technique with actual measurements of vertical noise coherence. For this purpose, data have already been collected at a few sites on the Scotian Shelf, mainly at Western Bank. Model-data comparisons, as well as an evaluation of the method will be presented in a future report.

TABLE OF CONTENTS

Section **Page**

Abstract ii
Résumé ii
Executive Summary iii
Table of Contents v
List of Figures vi
List of Tables vii
1. Introduction 1
2. The model 1
    2.1 Basic equations 1
    2.2 Addition of sea-water absorption 6
    2.3 Addition of a sound-speed profile in the water 9
3. Model sensitivity 10
    3.1 Sea-water absorption 11
    3.2 Bottom parameters 11
    3.3 Bottom layers 18
    3.4 Sound-speed profile 20
    3.5 Source directivity 23
4. Model strengths and weaknesses 25
5. Conclusions 27
References 28

LIST OF FIGURES

Figure **Page**

1. Reflection loss as a function of grazing angle for the six bottom types listed in Table 1. A: solid line; B: short-dashed line; C: long-dashed line; D: long-dash, dot; E: short-dash, dot; F: very long dashed line. 4

2. Relative intensity as a function of angle for the six bottom types listed in Table 1. A: solid line; B: short-dashed line; C: long-dashed line; D: long-dash, dot; E: short-dash, dot; F: very long dashed line. 4

3. Coherence (real part above, imaginary part offset by -1) as a function of *kd* for the six bottom types listed in Table 1. A: solid line; B: short-dashed line; C: long-dashed line; D: long-dash, dot; E: short-dash, dot; F: very long dashed line. 5

4. Relative intensity as a function of angle for the six bottom types listed in Table 1, water attenuation included. A: solid line; B: short-dashed line; C: long-dashed line; D: long-dash, dot; E: short-dash, dot; F: very long dashed line. 7

5. Coherence (real part above, imaginary part offset by -1) as a function of *kd* for the six bottom types listed in Table 1, water attenuation included. A: solid line; B: short-dashed line; C: long-dashed line; D: long-dash, dot; E: short-dash, dot; F: very long dashed line. 8

6. Upward refracting sound speed profile. Energy between 0° and θ_r does not interact with the bottom. 10

7. Downward refracting sound speed profile. Energy in the gray zone does not interact with sea surface. 10

8. Reflection loss as a function of grazing angle for frequencies of 100 to 1100 Hz, in steps of 100 Hz; the arrow indicates direction of change for increasing frequencies. 12

9. Relative intensity as a function of angle for frequencies of 100 to 1100 Hz, in steps of 100 Hz; the arrow indicates direction of change for increasing frequencies. 12

10. Coherence (real part above, imaginary part offset by -1) as a function of *kd* for frequencies of 100 to 1100 Hz, in steps of 100 Hz; the arrow indicates direction of change for increasing frequencies. 13

11. Reflection loss as a function of grazing angle for Sable Island sand (solid line), tertiary bedrock (short-dashed line), and tertiary bedrock with no shear wave (long-dashed line). 16

12. Relative intensity as a function of angle for Sable Island sand (solid line), tertiary bedrock (short-dashed line), and tertiary bedrock with no shear wave (long-dashed line). 16

13. Coherence (real part above, imaginary part offset by -1) as a function of *kd* for Sable Island sand (solid line), tertiary bedrock (short-dashed line), and tertiary bedrock with no shear wave (long-dashed line). 17

14. Coherence (real part above, imaginary part offset by -1) as a function of *kd* for Sable Island Sand over tertiary bedrock; sand layer thickness increases (in the direction of the arrow) from 5 to 50 m, in steps of 5 m. 19

15. *kd* value for first 0 crossing of real coherence as a function of layer thickness. 20

16. Isospeed profile (solid line); downward refracting profile (short-dashed line); upward refracting profile (long-dashed line); duct (dotted line). 21

17. Relative intensity as a function of angle over bottom type A for an isospeed profile (solid line); downward refracting profile (short-dashed line); upward refracting profile (long-dashed line); duct (dotted line). 21

18. Coherence (real part above, imaginary part offset by -1) as a function of *kd* over bottom type A for an isospeed profile (solid line); downward refracting profile (short-dashed line); upward refracting profile (long-dashed line); duct (dotted line). 22

19. Relative intensity as a function of angle over bottom type F for an isospeed profile (solid line); downward refracting profile (short-dashed line); upward refracting profile (long-dashed line); duct (dotted line). 23

20. Coherence (real part above, imaginary part offset by -1) as a function of kd over bottom type F for an isospeed profile (solid line); downward refracting profile (short-dashed line); upward refracting profile (long-dashed line); duct (dotted line). 24

21. Source directivity for a dipole source (solid line) and a monopole source (dashed line). 25

22. Coherence (real part above, imaginary part offset by -1) as a function of *kd* over bottom type B for dipole sources (solid line) and monopole sources (dashed line). 26

LIST OF TABLES

Table **Page**

1. Acoustic properties of example seabeds. The subscript p refers to the compressional wave, the subscript s to the shear wave. 6

2. Acoustic properties at Western Bank. The subscript p refers to the compressional wave, the subscript s to the shear wave. 14

3. Impact of bottom parameters on real and imaginary part of the coherence. The qualitative impact scale goes from 1 (not very important) to 4 (important). The subscript p refers to the compressional wave, the subscript s to the shear wave. 15

1. Introduction

The use of ambient noise to extract environmental information is particularly advantageous since it is ever-present in the ocean. It has already been shown that some seabed properties can be extracted from the spatial characteristics of the ambient noise field. Buckingham and Jones [1], for example, have estimated the compressional sound speed of surficial sediment from the structure of the vertical directionality of the noise field. Carbone *et al.* [2] have estimated both the compressional and shear speeds of the upper layers using vertical noise coherence measurements. The advantage of using noise coherence over noise directionality is that the former is an easier measurement: only two sensors are required, whereas a whole array of sensors is needed for the latter.

Chapman [3] developed a model to estimate the vertical ambient noise coherence in a simple shallow water environment. The approach is based on an energy flux propagation model. This report restates the original equations of the model, and extends it to include a multi-layered elastic seabed, sea-water absorption, and an arbitrary sound-speed profile in the water column. The method has the advantage of being simple yet allowing for a complicated environment without intensive numerical computations. Harrison [4] used a similar ray-based technique, and it was found to give results comparable to that of a full wave development.

The object of this report is to introduce the model and its latest modifications. Some comparisons with data are found in [3] and [5], and more will follow in a later report which will present an evaluation of the model. The basic equations are introduced in Section 2. Section 3 includes a sensitivity study to the following internal parameters: absorption by sea water, bottom parameters, sound-speed profile in the water column, and source directivity. The strengths and weaknesses of the model are discussed last.

2. The model

The coherence between two vertically separated sensors is calculated from the Fourier transform of the noise intensity at an underwater receiver as a function of vertical arrival angle. For frequencies of 100 Hz to 2000 Hz, the main noise source is usually wind or sea surface agitation. Cron *et al.* [6] have shown that surface noise sources are effectively dipoles at these frequencies. Cron and Sherman [7] and Cox [8] have shown how the surface source directivity relates to the noise directionality and spatial correlation at a receiver in the water column. Talham [9] went a step further by adding a seabed and sea-water absorption, and he calculated the noise directionality above a bottom mounted receiver. The technique presented here is based on the above references, but includes the contribution of noise from both above and below a receiver in the water column.

2.1 Basic equations

Starting with an isospeed environment of infinite depth, we can relate the noise received at a sensor within the water column to the noise radiated at the sea surface. Assuming a horizontally homogeneous distribution of mutually incoherent point sources at the sea surface (σ sources per

unit area), each radiating acoustic power P, we obtain an effective surface source strength of σP. The directivity function of each source is described as a dipole:

$$S(\theta) = 3\sin^2\theta, \tag{1}$$

where θ is the angle from the horizontal plane. The factor 3 normalizes the function so that

$$\int_0^1 \mathrm{d}(\sin\theta) S(\theta) = 1. \tag{2}$$

The received acoustic intensity (per unit solid angle) at the receiver is [8]:

$$I_0(\theta) = \frac{\sigma P}{2\pi}\frac{S(\theta)}{\sin\theta} \qquad (0 < \theta < \pi/2) \tag{3}$$

in which θ is positive above the horizontal plane. In the absence of reflections from the seabed, the received intensity is zero for negative angles. In the absence of absorption by sea water, the result is independent of the depth of the receiver: as the receiver depth is increased, the spherical loss within a unit solid angle is exactly compensated by the increase in the size of the contributing surface area.

We now add a plane seabed at depth H, parallel to the sea surface, with an intensity reflection coefficient $V_B(\theta)$ [a plane wave incident at grazing angle θ is reflected specularly at the same angle θ with its intensity reduced by the factor $V_B(\theta)$]. In this model, the reflection coefficient is obtained with the bottom reflectivity equations of Brekhovskikh [10], which allow for a complicated seabed with a layered structure[1]. The components $I_+(\theta)$ and $I_-(\theta)$ of the received intensity (from above and below the receiver respectively) are calculated from the intensity distribution $I_0(\theta)$ in the absence of reflections at the boundaries. Considering the reflection at the surface, the component $I_+(\theta)$ must be the sum of the distribution $I_0(\theta)$ and the reflection $I_-(\theta)$ from the surface:

$$I_+(\theta) = I_0(\theta) + V_S(\theta) I_-(\theta). \tag{4}$$

Similarly, the component $I_-(\theta)$ must be the reflection of $I_+(\theta)$ at the bottom:

$$I_-(\theta) = V_B(\theta) I_+(\theta). \tag{5}$$

These algebraic relations are easily solved to yield the solutions:

$$I_+(\theta) = I_0(\theta)\frac{1}{1 - V(\theta)}, \text{ and} \tag{6}$$

[1] Similarly, a surface reflection coefficient $V_S(q)$ can be included although in this report a pure reflection at the sea surface was used for all simulations.

$$I_{-}(\theta) = I_0(\theta)\frac{V_B(\theta)}{1-V(\theta)} \quad \text{,in which} \tag{7}$$

$$V(\theta) = V_S(\theta)V_B(\theta). \tag{8}$$

The measured noise level at the receiver is the integral over 4π steradians of $I(\theta)$, the noise intensity per unit solid angle, presuming the noise field is quasi-homogeneous. This last assumption is valid in shallow water if the receiver is away from the boundaries, and the frequency is not too low relative to the water depth. In terms of mean-squared pressure, the noise level is:

$$N = 2\pi Z_W \int_{-1}^{1} \mathrm{d}(\sin\theta) I(\theta) = \sigma P Z_W \int_{0}^{1} \mathrm{d}(\sin\theta) \frac{S(\theta)}{\sin\theta} \frac{1+V(\theta)}{1-V(\theta)} \tag{9}$$

in which Z_W is the acoustic impedance of sea water. The surface source strength σP depends on wind and wave conditions — an arbitrary value of unity is used in all simulations presented in this report.

The noise intensity profile calculated from Equations 6 and 7 is converted to noise coherence following the method of Cox [8]. The vertical noise coherence $\Gamma_v(k,d)$ is the normalized Fourier transform of the intensity:

$$\Gamma_v(k,d) = \int_{-1}^{1} \mathrm{d}(\sin\theta) I(\theta) e^{ikd\sin\theta} \Big/ \int_{-1}^{1} \mathrm{d}(\sin\theta) I(\theta). \tag{10}$$

where k is the acoustic wavenumber and d is the vertical separation between the two sensors. It should be noted that the factors σP will cancel out of this equation, i.e., the vertical coherence is independent of the surface source strength. Also for a multi-layered bottom, $V(\theta)$ will likely be frequency dependent as various wavelengths will interact differently with variable layer thicknesses. For a constant sensor separation, the function $\Gamma_v(k,d)$ needs to be evaluated independently for each frequency of interest.

To illustrate the results from the equations presented above, the examples of Chapman [3] are reproduced here. The examples are based on six different seabed types, described according to the parameters listed in Table 1. The bottom reflection loss as a function of grazing angle for each seabed type (calculated with Brekhovskikh [10]) is shown in Fig. 1. As the seabeds are assumed infinite in these cases, the reflection losses shown in Fig. 1 are independent of frequency. The relative intensity as a function of grazing angle (calculated with Equations 6 and 7) is shown in Fig. 2; an arbitrary value of σP=1 was used in these calculations. Note a discontinuity at 0° due to the theoretically null surface noise contribution at that angle. The real and imaginary parts of the coherence as a function of kd (calculated with Equation 10) are shown in Fig. 3 — the imaginary parts are offset by -1 relative to the real parts. A frequency of 100 Hz was used in these calculations. More detailed information on these examples is included in [3].

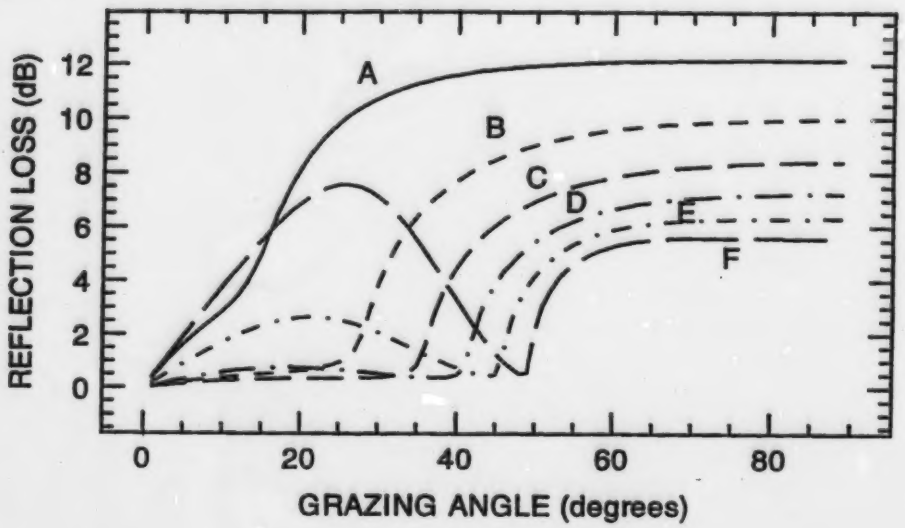

Figure 1. Reflection loss as a function of grazing angle for the six bottom types listed in Table 1. A: solid line; B: short-dashed line; C: long-dashed line; D: long-dash, dot; E: short-dash, dot; F: very long dashed line.

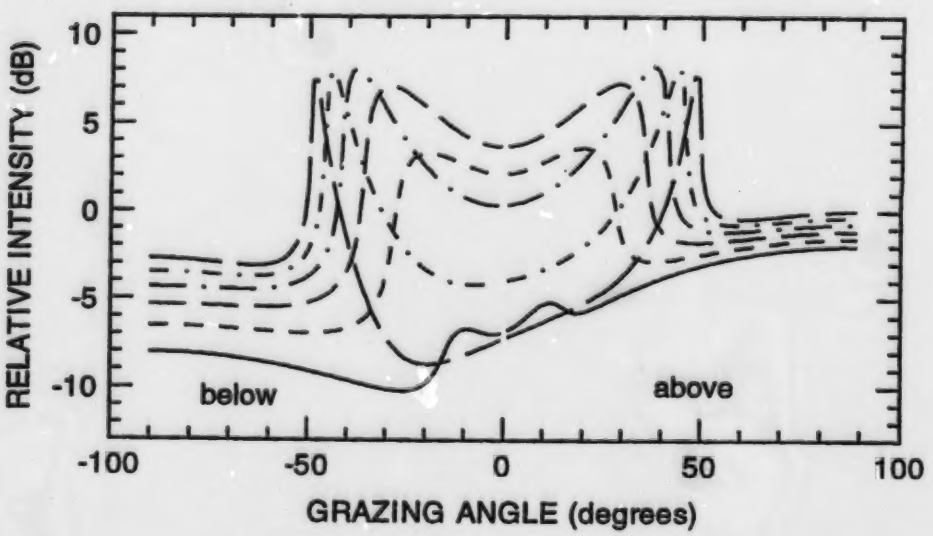

Figure 2. Relative intensity as a function of grazing angle for the six bottom types listed in Table 1. A: solid line; B: short-dashed line; C: long-dashed line; D: long-dash, dot; E: short-dash, dot; F: very long dashed line.

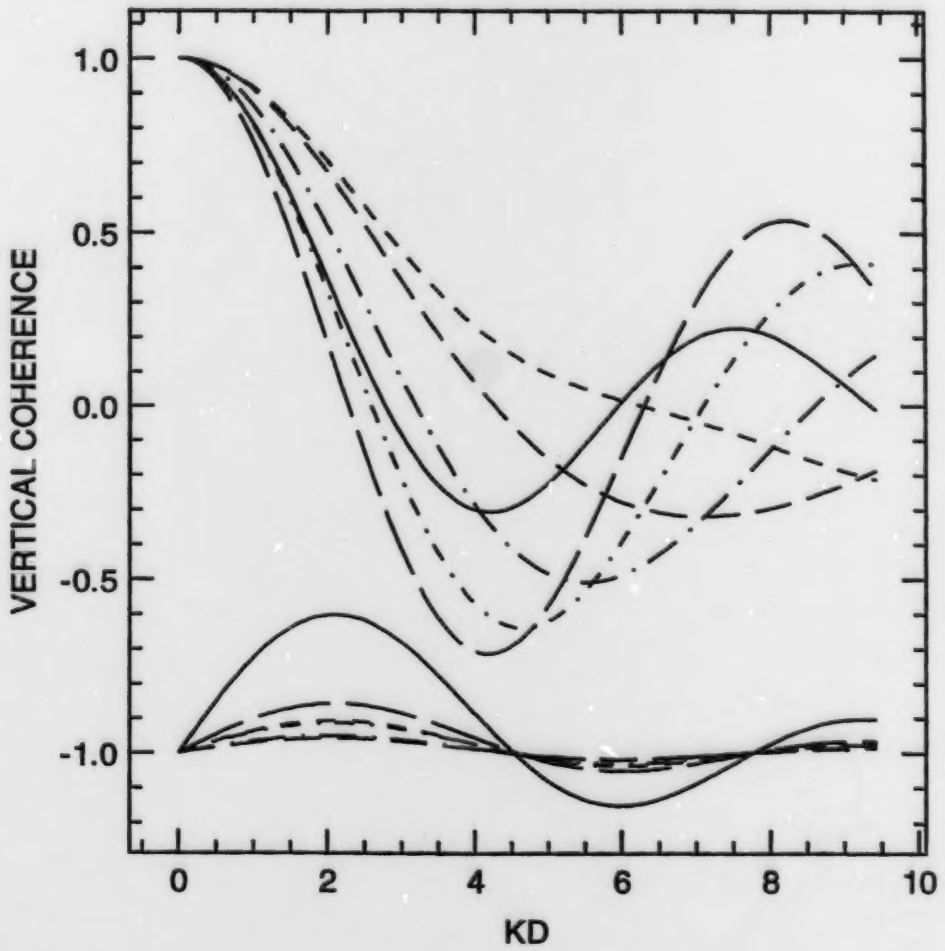

Figure 3. Coherence (real part above, imaginary part below offset by -1) as a function of *kd* for the six bottom types listed in Table 1. A: solid line; B: short-dashed line; C: long-dashed line; D: long-dash, dot; E: short-dash, dot; F: very long dashed line.

Table 1. Acoustic properties of example seabeds. The subscript p refers to the compressional wave, the subscript s to the shear wave.

Sediment label	Sediment description	Density (g/cm^3)	Sound speed (m/s)		Attenuation (dB/λ)		Critical angle (degrees)
		ρ	c_p	c_s	α_p	α_s	θ_c
A	silt	1.6	1550	125	0.78	0.25	14.6
B	fine sand	1.7	1700	200	0.60	0.25	28.1
C	coarse sand	1.8	1850	300	0.46	0.23	35.8
D	gravel	1.9	2000	450	0.40	0.23	41.4
E	glacial till	2.0	2150	650	0.32	0.20	45.8
F	soft sedimentary rock	2.1	2300	850	0.23	0.17	49.3

2.2 Addition of sea-water absorption

Absorption by sea water introduces a depth dependence which was previously absent in the equations of noise intensity. If the intensity of a plane wave drops to 1/e of its initial value over the distance $1/\alpha$, the corresponding absorption coefficient is 4.34α dB/unit distance. If we consider a semi-infinite medium, the noise arriving at angle θ at a receiver located at depth z has travelled a distance $z/\sin\theta$ from the surface, and the directionality function $I_0(\theta)$ must be multiplied by a factor $e^{-\alpha z/\sin\theta}$. The functions $I_+(\theta)$ and $I_-(\theta)$ become depth-dependent, and can be rewritten as follows:

$$I_+(\theta,z) = I_+(\theta,0)e^{-\alpha z/\sin\theta}, \text{ and} \tag{11}$$

$$I_-(\theta,z) = I_-(\theta,H)e^{-\alpha(H-z)/\sin\theta}, \tag{12}$$

where H is the water depth. Equations 4 and 5 are reformulated to take into account the new depth dependance:

$$I_+(\theta,0) = I_0(\theta) + V_s(\theta)I_-(\theta,0), \tag{13}$$

$$I_-(\theta,H) = V_B(\theta)I_+(\theta,H), \tag{14}$$

leading to the solutions:

$$I_+(\theta,0) = I_0(\theta)\frac{1}{1-V_{eff}(\theta)}, \tag{15}$$

$$I_{-}(\theta,H) = I_0(\theta)\frac{V_B(\theta)e^{-\alpha H/\sin\theta}}{1-V_{eff}(\theta)}, \tag{16}$$

in which

$$V_{eff}(\theta) = e^{-2\alpha H/\sin\theta}V_S(\theta)V_B(\theta). \tag{17}$$

As shown in the above equations, sea-water absorption introduces an effective reflection coefficient which is easily substituted in the intensity calculations. The absorption factor α is frequency-dependent, and was taken from [11].

The impact of sea-water absorption on the intensity distribution is shown in Fig. 4 for the same seabed types as in Figs. 1-3. The calculation was made at a frequency of 100 Hz (attenuation of 0.0045 dB/km). The main effect is seen near the horizontal (θ approaching 0°) where the acoustic paths from the surface to the receiver are longest. The original discontinuity at 0° (due to the theoretically null surface noise contribution at that angle) is broadened.

The impact on the real and imaginary parts of the coherence is minimal at this frequency, as seen by comparing Fig. 5 (coherence results with sea-water absorption included) to Fig. 3 (no sea-water absorption). More on this subject is presented in Section 3.1.

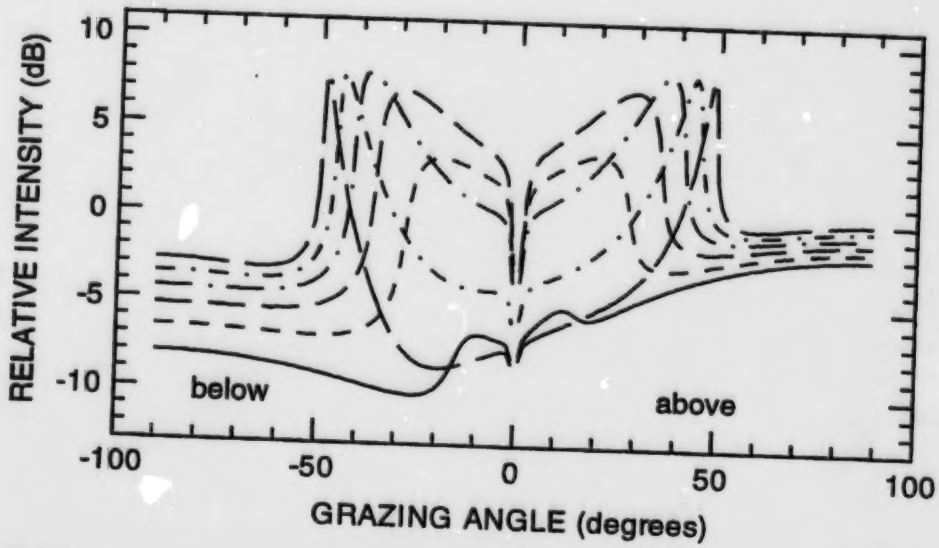

Figure 4. Relative intensity as a function of grazing angle for the six bottom types listed in Table 1, sea water absorption included. A: solid line; B: short-dashed line; C: long-dashed line; D: long-dash, dot; E: short-dash, dot; F: very long dashed line.

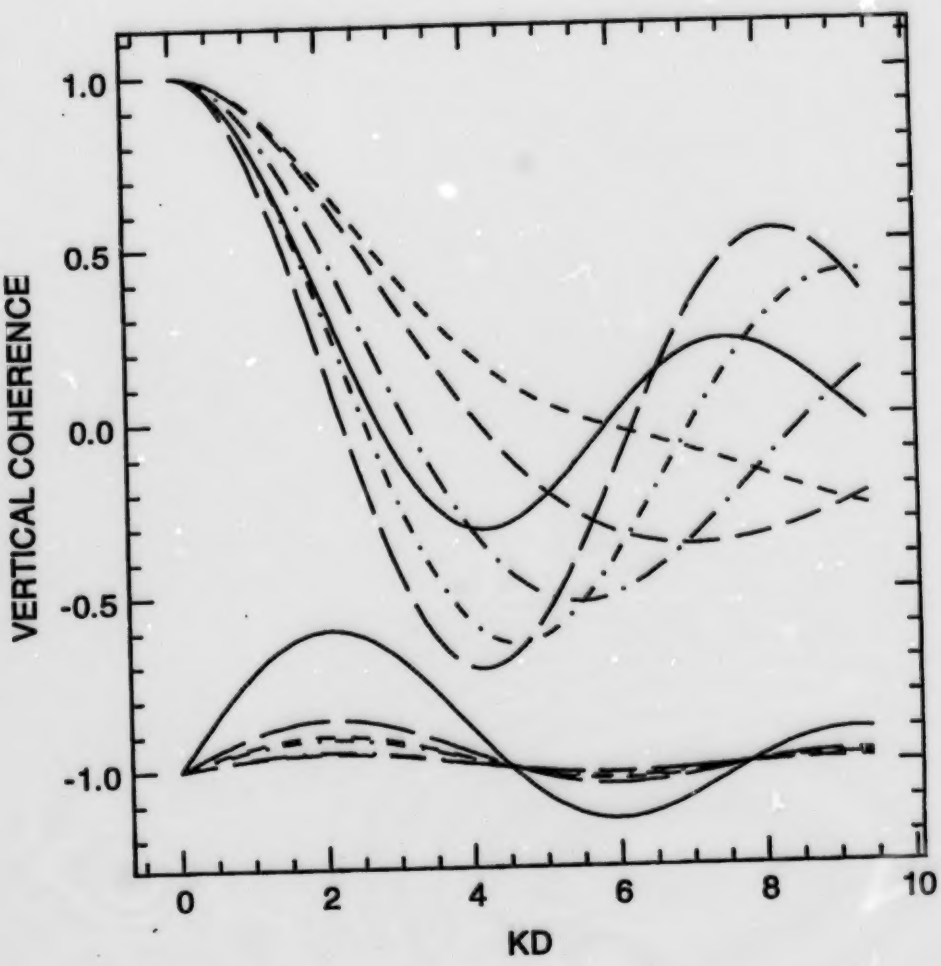

Figure 5. Coherence (real part above, imaginary part below offset by -1) as a function of *kd* for the six bottom types listed in Table 1, sea water absorption included. A: solid line; B: short-dashed line; C: long-dashed line; D: long-dash, dot; E: short-dash, dot; F: very long dashed line.

2.3 Addition of a sound-speed profile in the water

The introduction of a non-isospeed sound-speed profile in the water column has two main effects on the equations presented earlier:

- the path lengths from the sea surface to the receiver and from the sea bottom to the receiver can be elongated;
- the path angles at the sea surface and bottom correspond to different angles at the receiver.

The first effect changes Equations 11 and 12 to the following equations:

$$I_+(\theta_z,z) = I_+(\theta_0,0)e^{-\alpha z/\sin\theta_z} = I_+(\theta_0,0)e^{-\alpha L_+} \tag{18}$$

$$I_-(\theta_z,z) = I_-(\theta_H,H)e^{-\alpha(H-z)/\sin\theta_z} = I_-(\theta_H,H)e^{-\alpha L_-} \tag{19}$$

where L_+ and L_- are the path lengths for the energy coming from the boundaries above and below the receiver. The use of path lengths in this manner was justified by Harrison [4]. The angles θ_0, θ_H and θ_z refer to the grazing angles at the surface and bottom boundaries, and at the receiver depth respectively (these angles are now distinct because of the non-isospeed sound-speed profile). For receiver angles of -90° to +90°, the corresponding angles at the surface and bottom are found geometrically using Snell's law.

In the case of an isospeed profile: $\theta = \theta_0 = \theta_H$, $L_+ = z/\sin\theta$ (path length from the surface to the receiver) and $L_- = (H-z)/\sin\theta$ (path length from the bottom to the receiver). For an arbitrary sound-speed profile θ_0, θ_H, L_+ and L_- are estimated with a simple ray model. The parameters L_+ and L_- take into account the energy refraction introduced by the sound-speed profile. For example, in an upward refracting scenario, L_- at shallow angles is the path of acoustic energy coming from the sea surface and refracted upward below the receiver depth.

Equations 15 and 16 also change to reflect the new path lengths, and are rewritten as follows:

$$I_+(\theta_0,0) = \frac{I_0(\theta_0)}{\left[1 - V_S(\theta_0)V_B(\theta_H)e^{-2\alpha L_{total}}\right]} \tag{20}$$

$$I_-(\theta_H,H) = \frac{I_0(\theta_0)V_B(\theta_H)e^{-\alpha L_{total}}}{\left[1 - V_S(\theta_0)V_B(\theta_H)e^{-2\alpha L_{total}}\right]} \tag{21}$$

where L_{total} is the path length of the acoustic ray going from the sea surface to the sea bottom (or vice-versa).

When considering the path lengths L_+ and L_- in Equations 18 and 19, some particular cases have to be dealt with carefully. In the event of an upward sound-speed profile, as in Fig. 6, the rays

received at grazing angles between 0° and θ_r arrive from below the receiver, even though they originate from above the receiver. The angle θ_r is found through Snell's law [θ_r=cos^{-1}(sound speed at bottom/sound speed at receiver)]. For this small range of angles, Equation 19 has to be rewritten as:

$$I_-(\theta_z,z) = I_+(\theta_0,0)e^{-\alpha L_+}\ , \text{and similarly Equation (20) becomes:} \tag{22}$$

$$I_+(\theta_0,0) = \frac{I_0(\theta_0)}{\left[1 - V_s(\theta_0)e^{-\alpha L_{total}}\right]} \tag{23}$$

whereas Equations 18-21 remain valid for all other angles. Similarly, for a downward refracting sound-speed profile (as in Fig. 7), there will be a range of angles at the receiver (grey zone) for which the acoustic rays never interact with the surface. For these angles, $I_+(\theta_z,z)$ and $I_-(\theta_z,z)$ are equal to zero, resulting in a noise notch [11]. In a real environment, inhomogeneities in the medium would cause the edges of noise notch to be softened by ray leakage into the notch. This simple model does not account for this phenomenon.

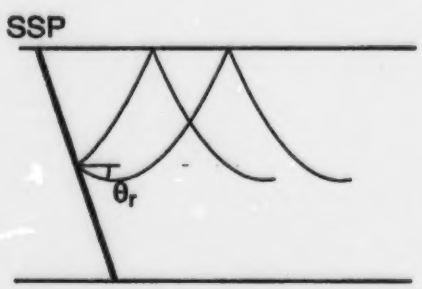

Figure 6. Upward refracting sound speed profile. Energy from ($0° < \theta < \theta_r$) does not interact with the bottom.

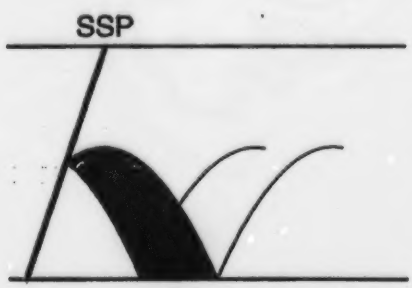

Figure 7. Downward refracting sound speed profile. Sea surface energy does not reach gray zone.

3. Model sensitivity

The following subsections will demonstrate the sensitivity of the model to the various internal parameters that control it. The effect of absorption by sea water is examined in more detail than in the previous section. The results of a sensitivity study on the various bottom parameters are included next, followed by a short discussion on bottom layers. The effect of an arbitrary sound-speed profile is then considered, followed by an overview of the effects of source directivity.

3.1 Sea-water absorption

The absorption by sea water is frequency-dependent. The effect is minimal at low frequency, and becomes gradually more important at frequencies above a few kHz. To quantify the effect, we will look at frequencies from 100 to 1100 Hz, in increments of 100 Hz.

Figure 8 shows the variation in the effective reflection loss (V_{eff} in Equation 17) as a function of grazing angle for these frequencies for bottom type C (recall Table 1). The effective reflection loss includes range effects through the path length term $z/\sin\theta$. As mentioned before, the effect is predominant at very low grazing angles, since the length of the acoustic path is greater for the energy travelling at shallow angles. Very little effect is seen above 10°. Below 10°, the effective reflection loss increases (in the direction of the arrow) with increasing frequency.

The corresponding relative intensity as a function of grazing angle is shown in Fig. 9, for the same frequencies. The intensity decreases with frequency (in the direction of the arrow), and again, the effect is more important at shallow grazing angles. Since the vertical coherence is an integration of the intensity, the real part of the coherence decreases with kd, as seen in Fig. 10 (in Fig. 10, an increase in kd implies an increase in d only as k — or the frequency — is constant for each individual curve). In other words, as the frequency increases (in the direction of the arrow), the coherence decreases more quickly with vertical separation.

3.2 Bottom parameters

A sensitivity study of the model over ocean bottom parameters was conducted to determine the effect of the various parameters on the real and imaginary parts of the vertical noise coherence. The effects are not always intuitive since the coherence of a noise field is more difficult to visualize than its vertical directionality. For this reason, it may be useful to first review some simple concepts.

For example, if a plane wave arrives at a grazing angle of 0° (horizontal wave), the signals recorded by two vertically separated hydrophones will be the same, leading to a real coherence of 1 for all combinations of hydrophone separations and frequencies (kd). If the same plane wave arrives from above or below the horizontal, the coherence will vary with both the hydrophone separation and/or frequency, in patterns similar to those presented so far in this report (e.g. Fig. 3). The more horizontal the field, however, the more slowly the vertical coherence will decay with kd. In a perfectly reflective environment, the contribution from above and below the receivers is the same, and the coherence is purely real. A vertical asymmetry in the field (from the different reflectivity of one of the boundaries for example) generates an imaginary component in the coherence field (the larger the vertical asymmetry in the field, the larger the imaginary component). This asymmetry in the field can be thought of as an asymmetry in the vertical energy flux [2].

The bottom profile shown in Table 2 was chosen for the sensitivity study — this bottom model is based on an area of Western Bank (Scotian Shelf) whose geology is well documented [12]. For the first part of the study, a simplified one-layer seabed of Sable Island sand (see Table 2) was used with an isospeed profile in the water. The bottom parameters were progressively changed

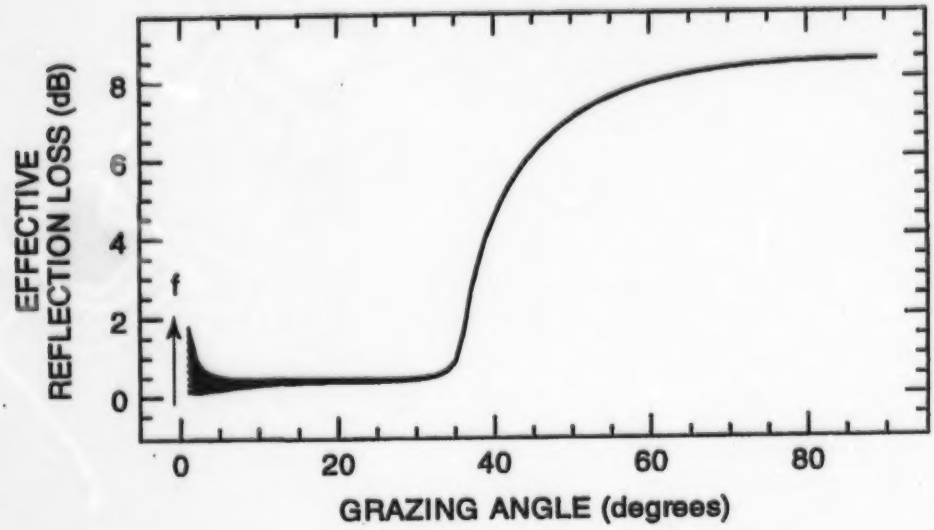

Figure 8. Effective reflection loss as a function of grazing angle for frequencies of 100 to 1100 Hz, in steps of 100 Hz; the arrow indicates direction of change for increasing frequencies.

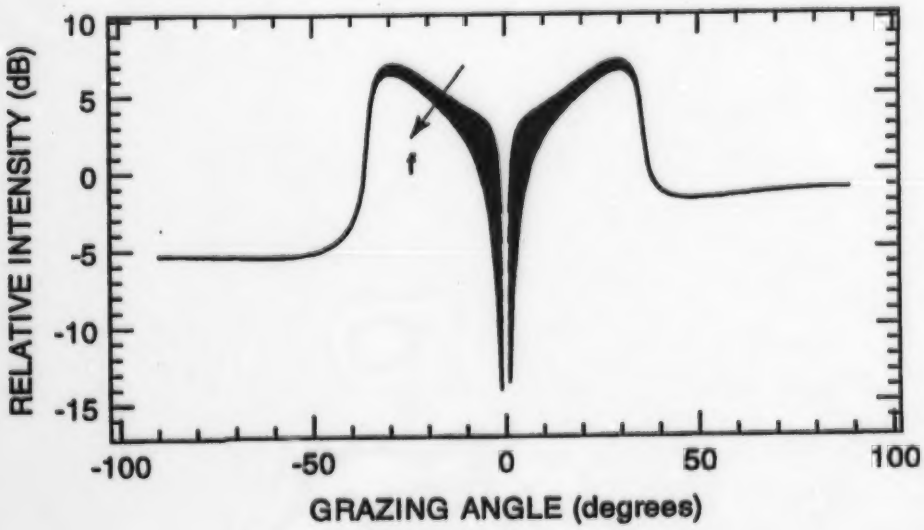

Figure 9. Relative intensity as a function of grazing angle for frequencies of 100 to 1100 Hz, in steps of 100 Hz; the arrow indicates direction of change for increasing frequencies.

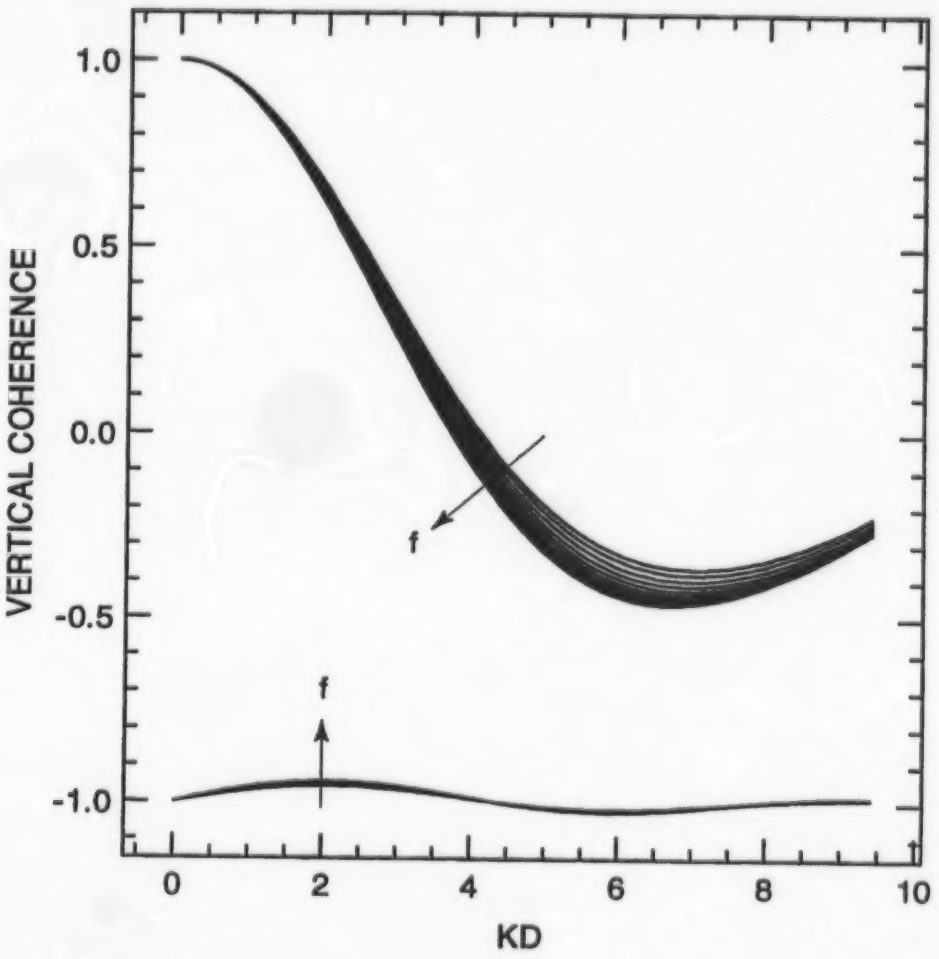

Figure 10. Coherence (real part above, imaginary part below offset by -1) as a function of *kd* for frequencies of 100 to 1100 Hz, in steps of 100 Hz; the arrow indicates direction of change for increasing frequencies.

Table 2. Acoustic properties at Western Bank. The subscript p refers to the compressional wave, the subscript s to the shear wave.

Sediment description	Density (g/cm^3)	Sound speeds (m/s)		Attenuations (dB/λ)		Thickness (m)
	ρ	c_p	c_s	α_p	α_s	z
water	1.0	1470	-	-	-	95
Sable Island sand and gravel	1.8	1650	260	0.46	1.3	37.5
till	2.1	1750	260	0.3	1.3	0-15
tertiary bedrock	2.2	2000	800	0.08	2.7	100

over a wide range of values, and the impact on the final coherence curves was noted. Similar variations were tried over a half-space of tertiary bedrock (as of Table 2), as well as combinations of sand layers of various thicknesses over a bedrock half-space.

The qualitative results of the study are summarized in Table 3. The individual bottom parameters are rated on an importance scale from 1 (not very important) to 4 (important). The scale is qualitative only, and indicates how large a change of the real and imaginary part of the coherence is produced by a variation of the parameters. The arrows in Table 3 give a quick reference on the behaviour of the coherence curves. For example, a downward arrow in the real coherence column of Table 3 indicates that the real part of the coherence will decay more rapidly as a function of *kd* as the value of the bottom parameter in question is increased. In the imaginary coherence column of Table 3, a downward arrow indicates that the amplitude of the imaginary part of the coherence will decrease as the value of the bottom parameter is increased. The goal of this exercise is to define which bottom parameters have the largest impact on the coherence and could potentially be inverted successfully from coherence masurements, and the qualitative scale fills this purpose adequately. As Table 3 is better discussed with specific examples, three sample cases were selected to clarify some of the effects.

The three sample cases are displayed in Figs. 11-13, and are as follows: the solid line represents the sand bottom as described in Table 2; the dashed line represents the case of a tertiary bedrock bottom; the long-dashed line represents the case of a bedrock bottom as for the dashed line case, but with zero shear speed (although unrealistic, this bottom type was added for comparison purposes). The individual bottoms were considered as half-spaces to produce Figs. 11-13, and the line type descriptions are identical in all three figures. The frequency was also constant at 100 Hz for these three cases, and an increase of *kd* implies an increase in *d*.

Figure 11 shows the reflection loss as a function of grazing angle for these three selected bottoms. The sand (solid curve) has the lowest critical angle (around 27°), and the highest reflection loss at high grazing angles. The bedrock (dashed curve) has a higher critical angle (around 43°), a

Table 3. Impact of bottom parameters on real and imaginary part of the coherence. The qualitative impact scale goes from 1 (not very important) to 4 (important). The subscript p refers to the compressional wave, the subscript s to the shear wave.

	Real coherence	Imaginary coherence	Comments
c_p	4 ↓	4 ↓	For higher c_p (and greater θ_c), energy propagates in a wider range of vertical angles
c_s	3 ↓	3 ↑	Loss of energy (p-wave to s-wave) between 0° and θ_c (important for high c_s)
α_p, α_s	1, 2 ↑	1,2 ↑	Effect greater near θ_c, asymmetry of field increases
ρ	1 ↓	2 ↓	Effect similar to that of c_p

high shear loss component around 20°, and lower loss than sand at high grazing angles. The no-shear bedrock (long-dashed curve) is similar to the bedrock bottom, without the shear loss at low grazing angles.

Figure 12 shows the relative intensity (σP taken as 1) as a function of grazing angle for the same three cases (the line types match those of Fig. 11). A discontinuity is seen at very low grazing angles for the near-horizontal paths that are attenuated most by sea-water absorption. The energy is concentrated at angles lower than the critical angle for each bottom type. A slightly higher intensity is seen for the positive angles (energy coming from above the receiver) due to the extra contribution from the direct paths from the sea surface (all the energy coming from below the receiver undergoes at least one bottom reflection because of the isospeed profile in the water). The intensity values at low grazing angles are very high for the no-shear bedrock (long-dashed curve) because of the low reflection loss at these angles, while the normal bedrock (dashed curve) shows the reverse effect. In fact, for the normal bedrock, only the narrow range of angles near the critical angle (43°) show significant intensity levels, as it is the only area with low reflection loss (see Fig. 11).

Figure 13 shows the real and imaginary part of the vertical coherence as a function of *kd*; the imaginary part is offset by -1. Again, the line types are matched to those of Figs. 11 and 12. The effect of a change in compressional sound speed is seen by comparing the curves for the sand bottom (solid line) and the no-shear bedrock (long-dashed line), for which the shear speeds are low. Since the harder bottom has a higher critical angle, the acoustic energy will be distributed over a wider range of angles in the vertical. At low shear speed, the imaginary part of the coherence is small, and the real part will decorrelate more quickly (over a shorter vertical distance) with a hard bottom.

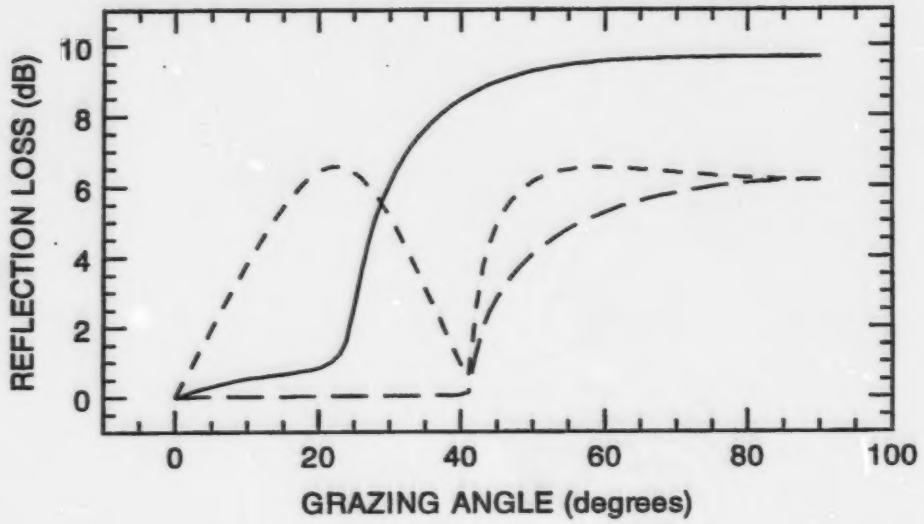

Figure 11. Reflection loss as a function of grazing angle for Sable Island sand (solid line), tertiary bedrock (short-dashed line), and tertiary bedrock with no shear wave (long-dashed line).

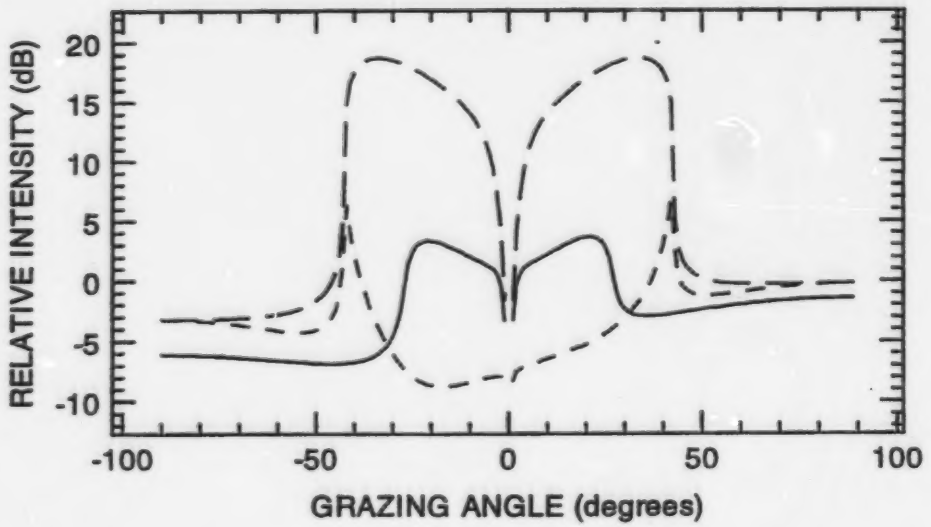

Figure 12. Relative intensity as a function of grazing angle for Sable Island sand (solid line), tertiary bedrock (short-dashed line), and tertiary bedrock with no shear wave (long-dashed line).

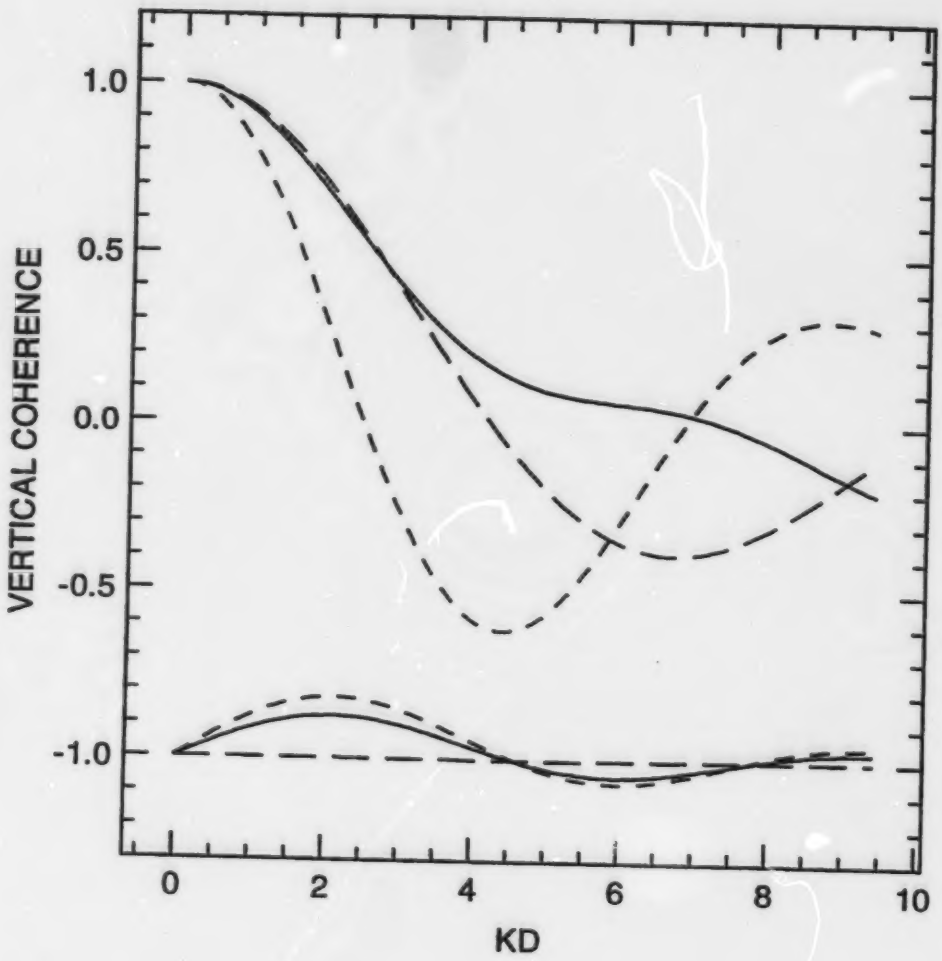

Figure 13. Coherence (real part above, imaginary part below offset by -1) as a function of *kd* for Sable Island sand (solid line), tertiary bedrock (short-dashed line), and tertiary bedrock with no shear wave (long-dashed line).

The effect of the shear speed is seen by comparing the normal bedrock (dashed line) and the no-shear bedrock (long-dashed line). The difference is greatest over the specific range of low grazing angles between 0° and θ_c (see Fig. 11). Over this range, part of the energy for the normal bedrock is converted from p-wave to s-wave, and the reflection loss gets higher. This loss translates to a higher imaginary part of the coherence (Fig. 13), and the real part decreases more quickly with vertical distance (or higher *kd*). It is important to note, however, that if the vertical coherence (particularly the imaginary part) is fairly sensitive to a change of shear speed *at high shear speeds*, the effect is benign at low shear speeds.

Changes in compressional or shear-speed attenuation have a lesser effect on the vertical coherence pattern. This point is not demonstrated with a specific figure, but the results of the sensitivity study are summarized in Table 3. As the energy interacts with a high attenuation seabed, the upward component of the noise field is reduced, and the asymmetry in the noise field increases. The impact is more visible on the imaginary part of the coherence which increases in amplitude. As for an increase in shear speed, the real part of the coherence decays more slowly with *kd* when the attenuation is increased. A change in density also has a lesser impact on the vertical coherence, with a final effect similar to a change in compressional sound speed: an increase in density will lower the amplitude of the imaginary part of the coherence, and induce a more rapid decay of the real part with *kd*.

3.3 Bottom layers

The presence of layers in the bottom introduces a frequency dependence in the reflection loss and coherence patterns. As sediment layers with different characteristics are combined, the final effect on the coherence curves can be very complicated, and it seems unlikely that the vertical coherence measurement could be used successfully to invert bottom properties past the first few layers.

A test was made with a simple two-layer case based on the Western Bank seabed of Table 2. The test seabed was made of a Sable Island sand layer of variable thickness overlying a tertiary bedrock half-space. An isospeed profile was assumed for the water. The sand layer was increased from 5 to 50 m, in steps of 5 m. The coherence curves for each thickness value are shown in Fig. 14; the arrows in Fig. 14 indicate the direction of change of the coherence as the layer thickness increases. For this case, there is little change in the imaginary part of the coherence for different layer thicknesses. The real part is also very similar once the thickness has increased to approximately 25 m. For layers thinner than about 25 m, the subbottom becomes more important, and will effectively increase the average impedance of the seabed. As a consequence, the real part of the coherence progressively decreases with *kd* as the layer gets thinner.

The *kd* value at which the real part of the coherence crosses zero was extracted from the curves in Fig. 14, and are shown in Fig. 15 as a function of the sand layer thickness. This plot confirms that the impact of the bedrock subbottom is important for very thin sand layers, but the effect progressively decreases, and the real part of the coherence stabilizes in this case for thicknesses above 35-40 m. If bottom inversion was attempted using vertical noise coherence, it is suspected

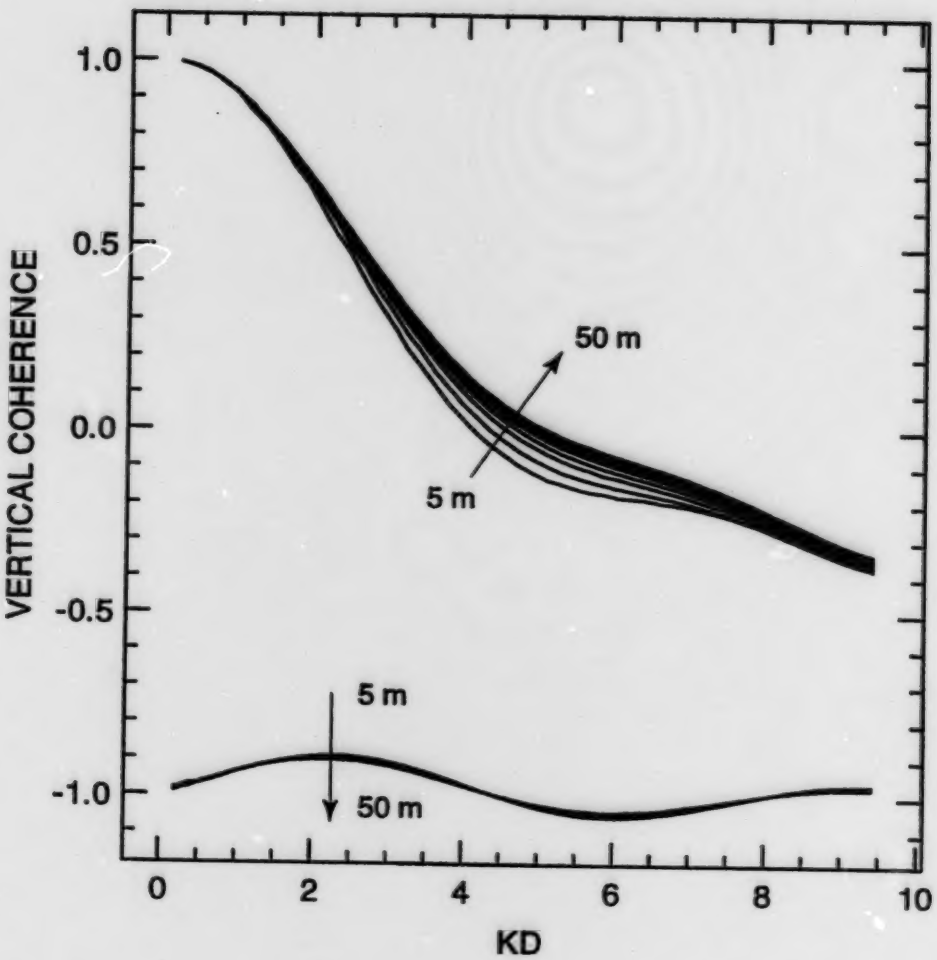

Figure 14. Coherence (real part above, imaginary part below offset by -1) as a function of *kd* for Sable Island Sand over tertiary bedrock; sand layer thickness increases (in the direction of the arrow) from 5 to 50 m, in steps of 5 m.

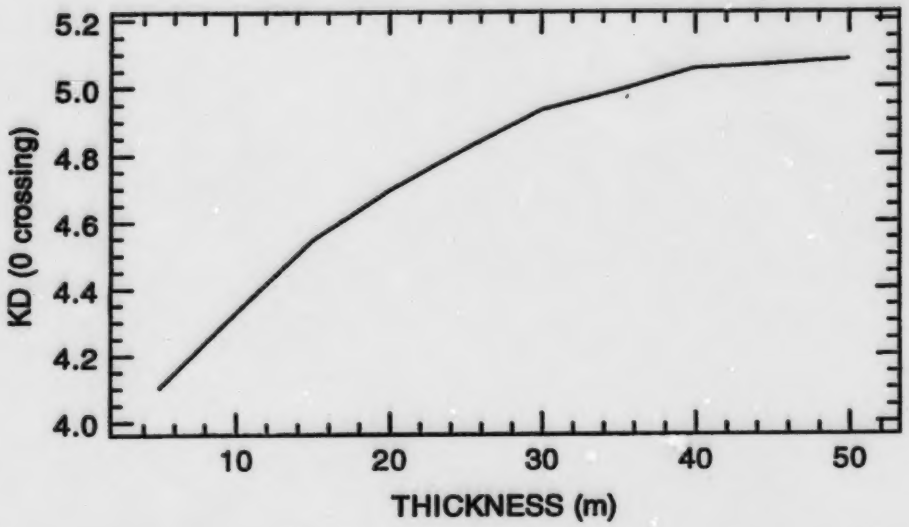

Figure 15. *kd* value for first zero crossing of real coherence as a function of layer thickness.

that the technique would lose sensitivity to bottom parameters below the first few tens of meters of sediment. Carbone *et al.* [2] reached a similar conclusion, although they were hoping that the next evolution of their inversion technique might succeed in resolving deeper layers by progressively homing in on them.

3.4 Sound-speed profile

The shape of the sound-speed profile can potentially have a large impact on the coherence curves. To demonstrate this point, four different sound-speed profiles are investigated, as shown in Fig. 16: an isospeed profile (solid line), a linear downward-refracting profile (short-dashed line), a linear upward-refracting profile (long-dashed line) and a duct (dotted line). A water depth of 100 m, and a receiver depth of 50 m were used in all three cases. Two different seabeds were selected: bottom A (silt) and F (soft sedimentary rock) from Table 1.

Figure 17 shows the relative intensity (dB) as a function of angle at the receiver with bottom A and for the four different sound-speed profiles (same line types as in Fig. 16). Positive angles are from above the receiver, negative angles are from below. The intensity curves are asymmetrical, higher noise contributions coming from above the receiver. The solid line reproduces the one in Fig. 4, as the input parameters to the model are the same in both cases. The outside of the humps near ±15° corresponds to the critical angle at the bottom (the angle varies slightly depending on the water sound speed at the seabed interface). In the case of a downward refracting profile (short-dashed line), we obtain a noise notch at ±6.6°, as no energy at angles shallower than $\pm\cos^{-1}(1510/1520)$ reaches the receiver. For an upward refracting profile (long-dashed line), lower losses at the seabed imply higher noise intensity near the horizontal. Energy at angles shallower than

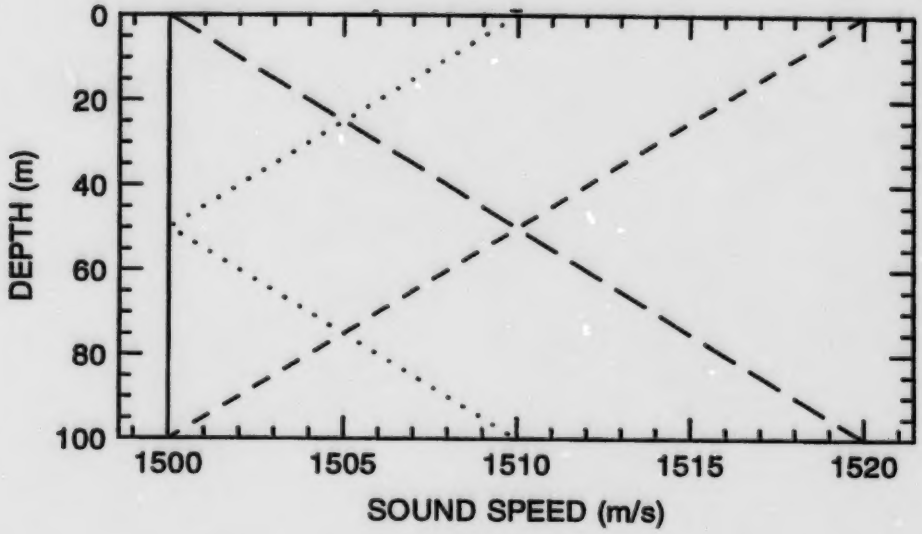

Figure 16. Isospeed profile (solid line); downward refracting profile (short-dashed line); upward refracting profile (long-dashed line); duct (dotted line).

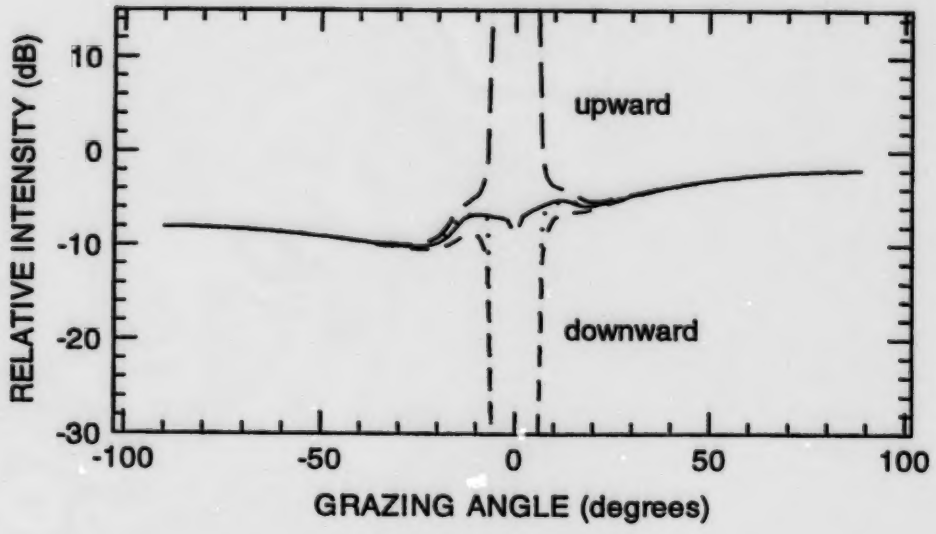

Figure 17. Relative intensity as a function of grazing angle over bottom type A for an isospeed profile (solid line); downward refracting profile (short-dashed line); upward refracting profile (long-dashed line); duct (dotted line).

±cos⁻¹(1510/1520) simply does not interact with the bottom, giving very large intensity levels (not infinite however, since water absorption has a small effect). In the case of a duct (dotted line), both effects are combined.

The normalized Fourier transform of the intensity curves of Fig. 17 (following Equation 10) gives the coherence curves (as a function of *kd*) of Fig. 18. In the upward refracting case (long-dashed line), the high intensity levels resulted in very high real coherence of the acoustic energy over large *kd* (or large vertical sensor separations). It also reduces markedly the imaginary part of the coherence, which is expected from the lesser acoustic interaction with the bottom. On the contrary, the downward refracting profile (short-dashed line) induces more bottom interactions, and leads to much lower coherence levels, or reduced vertical spatial correlation of the noise. The isospeed water (solid line) and the duct (dotted line) cases lie between the other two cases.

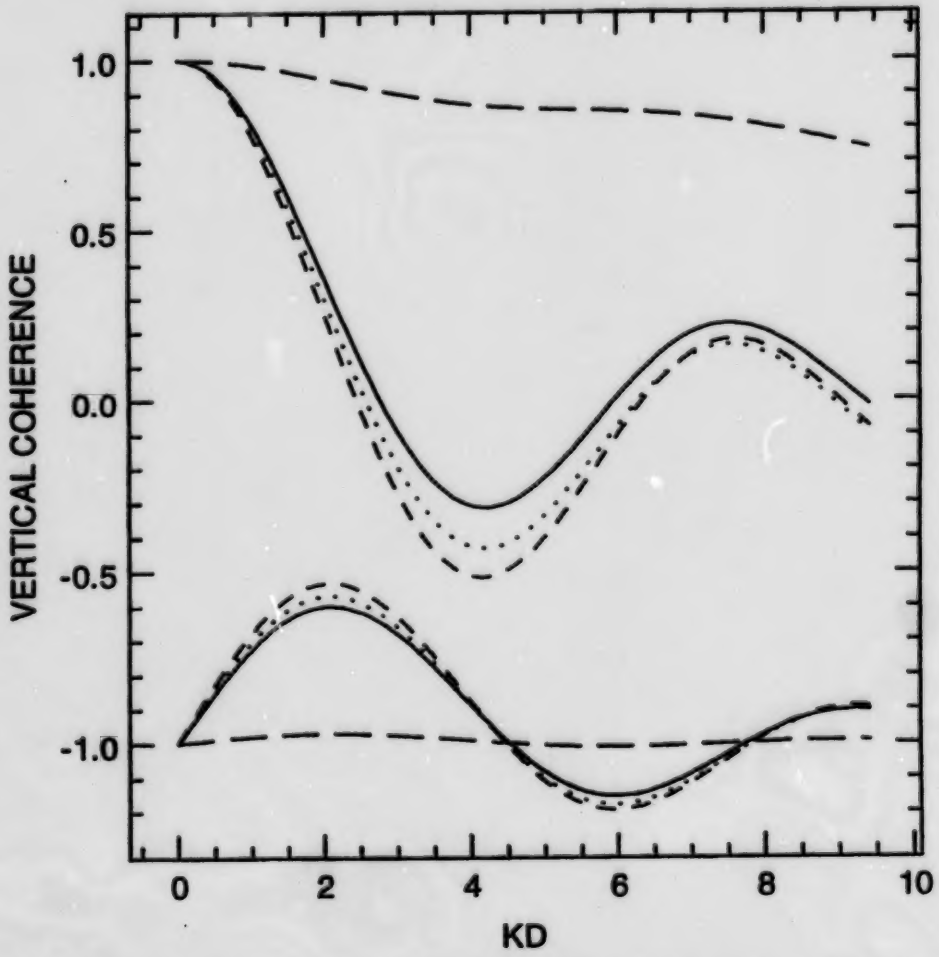

Figure 18. Coherence (real part above, imaginary part below offset by -1) as a function of *kd* over bottom type A for an isospeed profile (solid line); downward refracting profile (short-dashed line); upward refracting profile (long-dashed line); duct (dotted line).

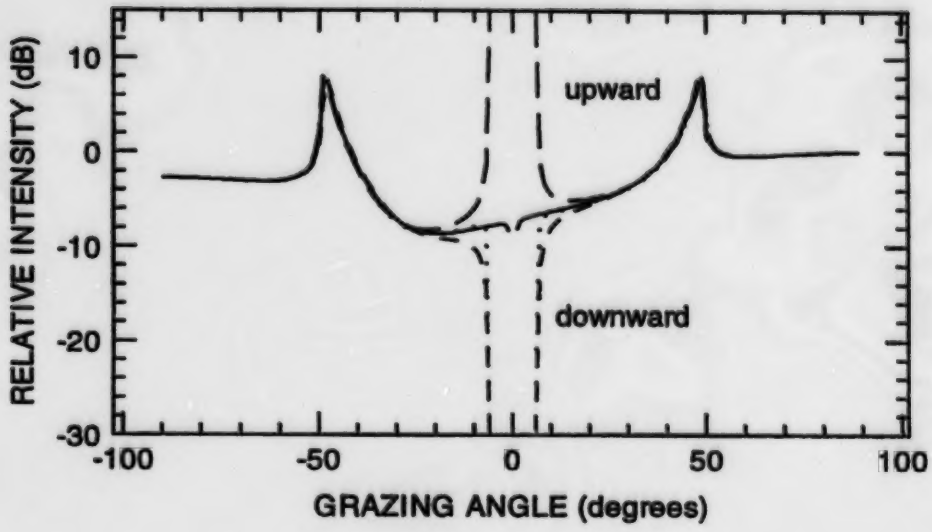

Figure 19. Relative intensity as a function of grazing angle over bottom type F for an isospeed profile (solid line); downward refracting profile (short-dashed line); upward refracting profile (long-dashed line); duct (dotted line).

The results for the sedimentary rock bottom (bottom F of Table 1) are shown in Fig. 19 (intensity plot) and Fig. 20 (coherence plot). The same line types are used for these two figures. The critical angle is much higher for this bottom (around 49°), as seen in Fig. 19. The impact of the noise notch (downward refracting and duct cases) is reduced as it affects angles where relatively little energy is propagating. Consequently, the coherence curves (Fig. 20) are very close for these three cases. The upward-refracting case, however, still has a strong impact since it shields the low-angle propagation from bottom interactions, and the real part of the coherence decays much more slowly.

3.5 Source directivity

From experimental data, Cron *et al.* [6] demonstrated that surface noise sources are effectively dipoles, unless nearby or distant shipping is a significant part of the background noise. Acoustic energy from shipping will mostly come from near horizontal angles. The model presented in this report does not have the option of adding a ship, but by changing the directivity of the surface noise sources, we can investigate the impact of near-horizontal energy on the coherence.

Figure 21 shows the downward directivity of the dipole pattern which is generally used to simulate wind generated surface noise sources (solid line), as well as the directivity of a monopole

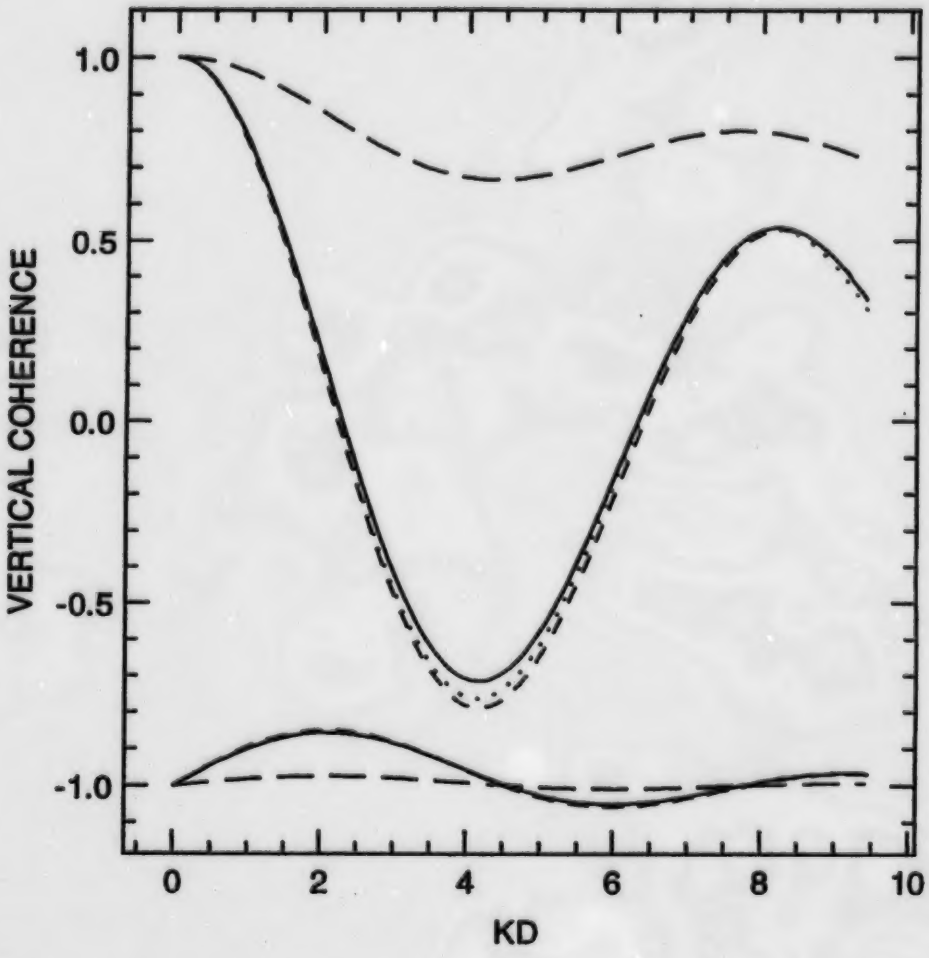

Figure 20. Coherence (real part above, imaginary part below offset by -1) as a function of kd over bottom type F for an isospeed profile (solid line); downward refracting profile (short-dashed line); upward refracting profile (long-dashed line); duct (dotted line).

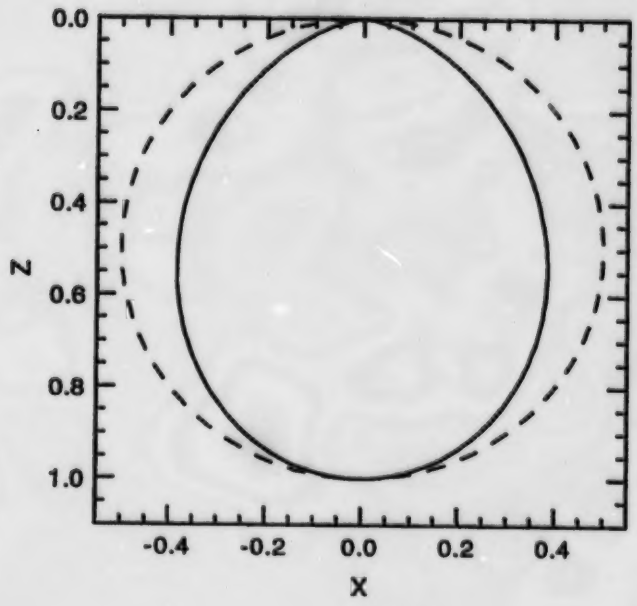

Figure 21. Source directivity for a dipole source (solid line) and a monopole source (dashed line).

source (dashed line). The monopole source directivity was modelled here as $S(\theta) = 3 \sin(\theta)$. The corresponding coherence curves using bottom B are shown in Fig. 22 (same line types). The monopole source directs more energy at near-horizontal angles, and this energy has a high level of vertical coherence. Consequently, the real part of the coherence effectively rises, while the imaginary part decreases (sign of a strong symmetry in the noise field).

Deane and Buckingham [13] used their normal-mode based model to calculate the vertical noise coherence from a ship. They represented the ship by the lowest-order (first) mode from a single, broadband surface source at a specific range, which they added incoherently to the wind surface sources. As the first mode represents acoustic energy propagating near-horizontally, their results were qualitatively the same, i.e., an increase in the real part of the coherence, and a decrease of the amplitude of the oscillations in the imaginary part.

4. Model strengths and weaknesses

The biggest strength of this model is by far its simplicity. Most effects from the ocean and seabed were included in the model without having recourse to the full wave equation. As a result, the model leads to realistic results at a very modest computational cost.

On the other hand, the biggest weakness of the model is the lack of range dependency. The model only uses the sound-speed profile to correct the arrival angles at the receiver, therefore only the sound speeds at the receiver and at the boundaries or at maxima above and below the receiver are used. If the environment changed in a 2-D or 3-D manner, a full-scale ray-model would have to

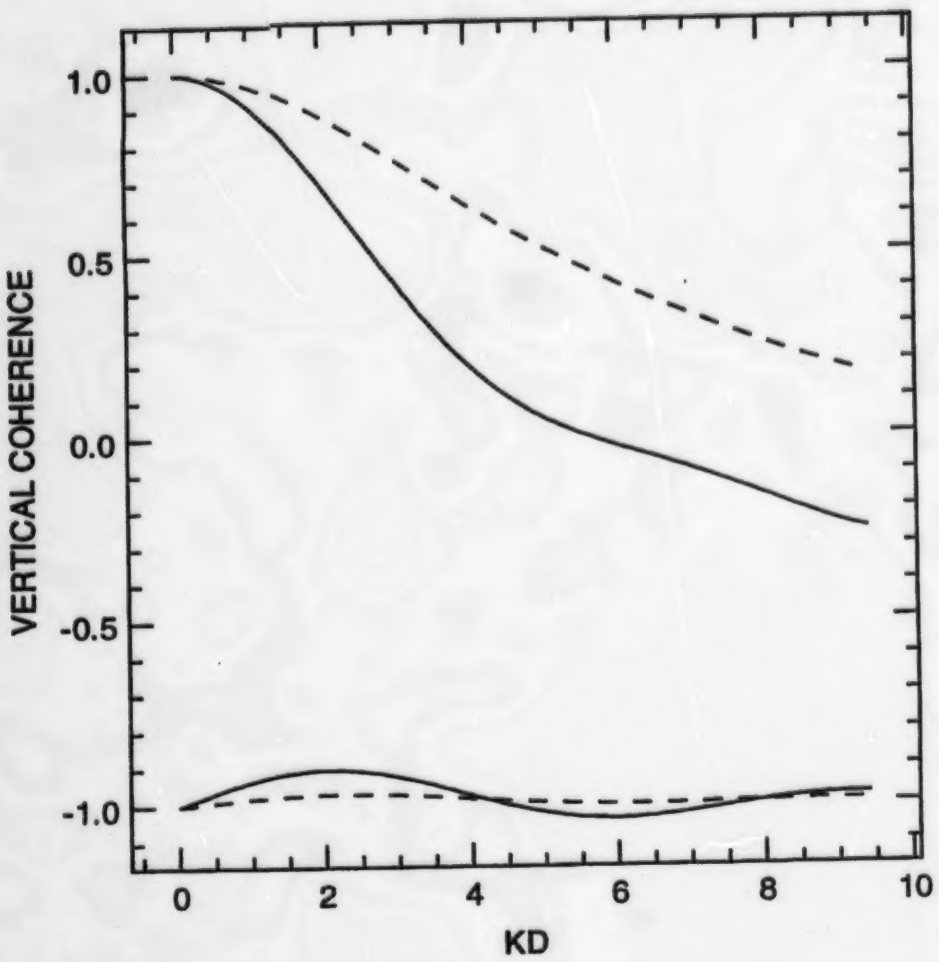

Figure 22. Coherence (real part above, imaginary part below offset by -1) as a function of *kd* over bottom type B for dipole sources (solid line) and monopole sources (dashed line).

be attached to the coherence model to extract the ray paths from the surface sources to the receiver, and the losses along these paths. This scenario would not be ideal for a shallow water environment.

Shipping sources are not included in this model, although it might be possible to mimic distant shipping by increasing the source level at near-horizontal angles.

5. Conclusions

We presented a simple model of vertical noise coherence, based on a uniform distribution of sources at the ocean surface, an energy flux propagation model, and a plane-wave bottom reflection coefficient for a multi-layered elastic seabed. The model also allows for sea-water absorption, and an arbitrary sound-speed profile in the water column.

The model can be used to infer seabed properties from coherence measurements. It was found that the compressional sound speed of the upper sediment layer has a strong influence on the vertical noise coherence, as well as the shear speed (if the shear speed is high to start with). Compressional and shear wave attenuations as well as bottom density have lesser effects on both the real and imaginary parts. Sediment layering can induce large changes in the vertical coherence. At depths greater than a few tens of meters within the seabed, the coherence becomes less sensitive to seabed properties, which become more difficult to invert.

The coherence is a normalized measurement, therefore the structure of the noise coherence is more sensitive to the seabed than to sea state conditions. However, the sound-speed profile in the water column, as in the seabed, has a directive effect on the noise spatial distribution, and can be very important, especially for upward-refracting profiles when bottom interactions are limited. Poor knowledge of the oceanographic environment can lead to poor estimates of seabed parameters.

Shipping effects were not modelled directly, but it was demonstrated that an increased source directivity near horizontal angles produces similar effects. Further research on this topic needs to be done before adding shipping noise to the model.

References

1. Buckingham, M.J. and Jones, S.A.S., A new shallow-ocean technique for determining the critical angle of the seabed from the vertical directionality of the ambient noise in the water column, J. Acoust. Soc. Am., 1987, **81**, 938-946.

2. Carbone, N.M., Deane, G.B. and Buckingham, M.J., The compressional and shear wave speeds of a seabed in shallow water determined from ambient noise measurements. In *Sea Surface Sound '94*, eds. M.J. Buckingham and J.R. Potter, World Scientific, Singapore, 1995, pp. 32-44.

3. Chapman, D.M.F., Surface-generated noise in shallow water: a model, Proc. Inst. of Acoust., 1987, **9**(4), 1-11.

4. Harrison, C.H., Formulas for ambient noise level and coherence, J. Acoust. Soc. Am., 1996, **99**, 2055-2066.

5. Desharnais, F. and Chapman, D.M.F., Modelling the vertical coherence of the shallow water ambient noise field. In *Sea Surface Sound '97*, T.G. Leighton ed., Print and Media Resources, Fordingbridge, Hampshire, UK, 1997, pp. 111-118.

6. Cron, B.F., Hassell, B.C. and Keltonic, F.J., Comparison of theoretical and experimental values of spatial correlation, J. Acoust. Soc. Am., 1965, **37**, 523-529.

7. Cron, B.F. and Sherman, C.H., Spatial-correlation functions for various noise models, J. Acoust. Soc. Am., 1962, **34**, 1732-1736.

8. Cox, H., Spatial correlation in arbitrary noise fields with application to ambient sea noise, J. Acoust. Soc. Am., 1973, **54**, 1289-1301.

9. Talham, R., Ambient-sea-noise model, J. Acoust. Soc. Am., 1964, **36**, 1541-1544.

10. Brekhovskikh, L.M., *Waves in Layered Media, 2nd Edition*, (Robert T. Beyer, transl.), Academic Press, London, 1980.

11. Jensen, F.B., Kuperman, W.A., Porter, M.B. and Schmidt, H., *Computational Ocean Acoustics*, AIP Press, New York, 1993.

12. Osler, J.C., A geo-acoustic and oceanographic description of several shallow water experimental sites on the Scotian Shelf, DREA Technical Memorandum 94/216, November 1994.

13. Deane, G.B. and Buckingham, M.J., Vertical coherence of ambient noise in shallow water overlying a fluid seabed, J. Acoust. Soc. Am., 1997, **102**, 3413-3424.

UNCLASSIFIED
SECURITY CLASSIFICATION OF FORM
(highest classification of Title, Abstract, Keywords)

DOCUMENT CONTROL DATA

(Security classification of title, body of abstract and indexing annotation must be entered when the overall document is classified)

1. ORIGINATOR (the name and address of the organization preparing the document.. Organizations for whom the document was prepared, e.g. Establishment sponsoring a contractor's report, or tasking agency, are entered in section 8.)

Defence Research Establishment Atlantic
PO Box 1012
Dartmouth, Nova Scotia, Canada B2Y 3Z7

2. SECURITY CLASSIFICATION (overall security classification of the document including special warning terms if applicable).

UNCLASSIFIED

3. TITLE (the complete document title as indicated on the title page. Its classification should be indicated by the appropriate abbreviation (S,C,R or U) in parentheses after the title).

Vertical coherence of the shallow water ambient noise field, a model

4. AUTHORS (Last name, first name, middle initial. If military, show rank, e.g. Doe, Maj. John E.)

Francine Desharnais and David M.F. Chapman

5. DATE OF PUBLICATION (month and year of publication of document)

Feb 1999

6a. NO .OF PAGES (total containing information Include Annexes, Appendices, etc).

31 (approx.)

6b. NO. OF REFS (total cited in document)

13

7. DESCRIPTIVE NOTES (the category of the document, e.g. technical report, technical note or memorandum. If appropriate, enter the type of report, e.g. interim, progress, summary, annual or final. Give the inclusive dates when a specific reporting period is covered).

TECHNICAL MEMORANDUM

8. SPONSORING ACTIVITY (the name of the department project office or laboratory sponsoring the research and development. Include address).

Defence Research Establishment Atlantic

9a. PROJECT OR GRANT NO. (if appropriate, the applicable research and development project or grant number under which the document was written. Please specify whether project or grant).

Project 1CA11

9b. CONTRACT NO. (if appropriate, the applicable number under which the document was written).

10a ORIGINATOR'S DOCUMENT NUMBER (the official document number by which the document is identified by the originating activity. This number must be unique to this document.)

DREA TM 1999-011

10b OTHER DOCUMENT NOs. (Any other numbers which may be assigned this document either by the originator or by the sponsor.)

11. DOCUMENT AVAILABILITY (any limitations on further dissemination of the document, other than those imposed by security classification)

(X) Unlimited distribution
( ) Defence departments and defence contractors; further distribution only as approved
( ) Defence departments and Canadian defence contractors; further distribution only as approved
( ) Government departments and agencies; further distribution only as approved
( ) Defence departments; further distribution only as approved
( ) Other (please specify):

12. DOCUMENT ANNOUNCEMENT (any limitation to the bibliographic announcement of this document. This will normally correspond to the Document Availability (11). However, where further distribution (beyond the audience specified in (11) is possible, a wider announcement audience may be selected).

UNCLASSIFIED, UNLIMITED

DCD03 2/06/87-M/ DREA mod. 17 Dec 1997

13. ABSTRACT (a brief and factual summary of the document. It may also appear elsewhere in the body of the document itself. It is highly desirable that the abstract of classified documents be unclassified. Each paragraph of the abstract shall begin with an indication of the security classification of the information in the paragraph (unless the document itself is unclassified) represented as (S), (C), (R), or (U). It is not necessary to include here abstracts in both official languages unless the text is bilingual).

A shallow water noise model is used to simulate the vertical coherence of an acoustic noise field due to sea surface noise. The coherence between two vertically separated sensors is calculated from the Fourier transform of the received noise intensity as a function of vertical arrival angle. The vertical noise directionality is derived from a uniform distribution of sources at the ocean surface, an energy flux propagation model and a plane-wave bottom reflection coefficient for a multi-layered elastic seabed. The propagation model allows for an arbitrary sound speed profile in the water column and includes sea water absorption. This simple model clearly demonstrates the influence of seabed parameters, sound speed profile in the water, and noise source directivity on the vertical coherence of the noise field.

14. KEYWORDS, DESCRIPTORS or IDENTIFIERS (technically meaningful terms or short phrases that characterize a document and could be helpful in cataloguing the document. They should be selected so that no security classification is required. Identifiers, such as equipment model designation, trade name, military project code name, geographic location may also be included. If possible keywords should be selected from a published thesaurus. e.g. Thesaurus of Engineering and Scientific Terms (TEST) and that thesaurus-identified. If it not possible to select indexing terms which are Unclassified, the classification of each should be indicated as with the title).

Vertical coherence, shallow water, ambient noise, acoustic model, sea surface noise